Int J Cardiovasc Imaging (2015) 31:11–19
DOI 10.1007/s10554-014-0521-x

ORIGINAL PAPER

Determination of culprit coronary artery branches using hemodynamic indices from angiographic images

Zhang Zhang · Jun Chen · Shigeho Takarada · Sabee Molloi

Received: 9 June 2014 / Accepted: 12 August 2014 / Published online: 7 October 2014

Abstract A recently reported angiographic technique for hemodynamic indices based on first-pass distribution analysis (FPA) could potentially be helpful for determining the culprit artery responsible for myocardial ischemia. The purpose of this study was to determinate the culprit coronary arterial branches based on coronary flow reserve (CFR) and fractional flow reserve (FFR) using only angiographic images. The study was performed in 14 anesthetized swine. Microspheres were injected into coronary arterial branches to create microvascular disruption. Stenosis was also created by inserting plastic tubings in LAD and LC_X arterial branches. Adenosine was used to produce maximum hyperemia. Angiographic CFR (CFR_a), relative angiographic CFR ($rCFR_a$), and angiographic FFR (FFR_a) were calculated by FPA. The diagnostic abilities of CFR_a, $rCFR_a$, and FFR_a were compared in three models: (1) epicardial stenosis model (S), (2) microcirculation disruption model (M), and (3) combined(S + M) model by using the area under the ROC curve (AUC). The mean differences between FFR_a and the pressure-derived FFR (FFR_p) measurements were -0.01 ± 0.21 in S model (N = 37) and 0.01 ± 0.18 in M model (N = 53). From 225 measurements in S model, the AUCs for CFR_a and FFR_a were 0.720 and 0.918, respectively. From 262 measurements in M model and 238 measurements in (S + M) model, the AUCs for CFR_a, $rCFR_a$, FFR_a were 0.744, 0.715, 0.959 and 0.806, 0.738, 0.995, respectively. The hemodynamic indices of the small branches (down to $\sim$0.7 mm) could be measured using only angiographic image data. The application of FFR_a could potentially provide a useful method to assess the severity of disease in coronary arterial branches.

Keywords Angiography · Blood flow · Coronary disease · Fractional flow reserve · Coronary flow reserve

Z. Zhang · J. Chen · S. Molloi (✉)
Department of Radiological Sciences, School of Medicine, Medical Sciences I, B-140, University of California-Irvine, Irvine, CA 92697-5000, USA
e-mail: symolloi@uci.edu

Z. Zhang
Department of Radiology, Tianjin Medical University General Hospital, Tianjin 300052, China

S. Takarada · S. Molloi
Department of Medicine (Cardiology), University of California-Irvine, Irvine, CA 92697, USA

Introduction

Many cardiac hemodynamic indices could be measured by using a sensor-tipped guidewire to determine the culprit coronary arteries which relate to the corresponding myocardial ischemia [1]. However, a widespread implementation of the routine sensor-tipped guidewire techniques has been hampered by several factors including its complexity, invasiveness, and expense. It is still not feasible to complete all the wire measurements in order to get a good understanding of the coronary physiological status for every patient, especially in the case of small branches. It would be best to have a single diagnostic technique that can determine the culprit coronary artery with both anatomic and physiological information using only angiographic image data [2].

Previous studies have validated that coronary flow reserve (CFR) and fractional flow reserve (FFR) can be measured by using the angiographic images based on the first-pass distribution analysis (FPA) concept [3, 4]. The purpose of this study was to measure CFR and FFR in

coronary arterial branches based on angiographic images in order to assess both global and regional physiological condition of the coronary artery circulation.

Methods

Protocol

In a close-chest swine model, CFR and FFR measurements were performed at various stages of severity of microvascular abnormality and stenosis in left anterior descending (LAD) and left circumflex coronary artery (LC_X) based on FPA branches. Pressure derived FFR measurements were performed at various severities of coronary artery disease by pressure wire. The study protocol was approved by the University of California-Irvine Institutional Animal Care and Use Committee.

Animal preparation

Fourteen fasted domestic Yorkshire swine (37.6 ± 6.4 kg, male, S&S Farms) were sedated and pre-medicated with Telazol–ketamine–xylazine (4.4, 2.2, and 2.2 mg drug/kg body weight, respectively) and atropine (0.05 mg kg^{-1}). Anesthesia was maintained with 1–2 % isoflurane (Highland Medical Equipment Vaporizer; Temecula, CA, USA), and supplemental oxygen was provided via endotracheal intubation. Sheaths were placed in the carotid artery and jugular vein. Each swine was positioned on its right side under a flat panel detector. An intravenous drip of adenosine (400 μg kg^{-1} min^{-1}) was used to induce maximum hyperemia. Electrocardiogram, arterial blood pressure, X-ray pulse signal, and other relative physiological parameters were continuously recorded (MP100, Biopac Systems; Santa Barbara, CA, USA).

Catheterization

Heparin was administered (10,000 U bolus followed by additional 4,000–5,000 U per h) before catheterization. The left main ostium was cannulated with a 6-Fr hockey-stick catheter through the left carotid artery under fluoroscopic guidance. Another 4-Fr hockey-stick catheter was placed in the right atrium to measure the coronary venous pressure. A guidewire was placed in the target artery through the catheter, and then a micro-catheter was inserted in the target artery. Microcirculation was disrupted by injecting 1 ml of 50–100 μm (1.8×10^4 microspheres/ml) microspheres (Polysciences; Warrington, PA, USA) at a time in the branch through the micro-catheter [5]. This procedure was repeated several times for different degrees of severity of microcirculatory embolism. A heparin-coated polyurethane tubing (0.030″ ID × 0.065″ OD, Strategic Applications Inc; CA) was push over the guidewire to the branch with micro-catheter in order to create a local stenosis. Angiography was used to ensure the position of tubing. An intracoronary pressure wire (Radi Medical System, 0.014 in.) was advanced into the distal segment of the stenosis to measure the distal coronary pressure.

Image acquisition and processing

All images were acquired using a conventional X-ray tube with a constant potential X-ray generator (Optimus M200, Philips Medical Systems, Shelton, CT, USA). A cesium iodide-based flat panel detector (PaxScan 4030A, Varian Medical, Palo Alto, CA, USA) was used for image acquisition. The flat panel detector has a 40 × 30 cm^2 field of view and pixel size of 0.194 × 0.194 mm^2. The zoom-center mode was used to acquire images with 1,024 × 768 pixels. Gain and flat-field corrections were performed before image acquisition. Images were acquired at 30 frames per second. All images were corrected for X-ray scatter before logarithmic transformation. Publicly available software (ImageJ, National Institutes of Health, Bethesda, MD, USA) was used for image analysis. Pancuronium (0.1 mg kg^{-1}) was administered intravenously. Contrast material (Omnipaque-350, Princeton, NJ, USA) was power injected (Leibel-FlarsheimAngiomat 6000, Cincinnati, OH, USA) at 3 ml s^{-1} for 3 s. Coronary angiograms were acquired in both baseline and hyperemia conditions. The ventilator was turned off at the end of a full expiration to minimize respiratory motion. An image of a calibration phantom positioned over the heart was also acquired to determine the correlation between image gray level and iodine mass. Correction was made for differential magnification of the phantom and the heart [6, 7].

Blood flow measurement using angiographic images

We have previously reported that the FPA analysis technique can be used to measure absolute coronary blood flow by analyzing the propagation of a contrast material signal in the coronary system [8]. A region of interest (ROI) for flow measurement was drawn around the vascular bed that encompassed both the visible arteries and the microcirculatory blush (Fig. 1). Power injection of contrast material was assumed to momentarily replace blood with the contrast material. The known iodine concentration in the contrast material and a linear regression analysis between the measured integrated gray levels in the calibration phantom were used to convert the gray level to volume. The ratio of the measured volume change to the time period of the cardiac cycle yields volumetric coronary blood flow [9].

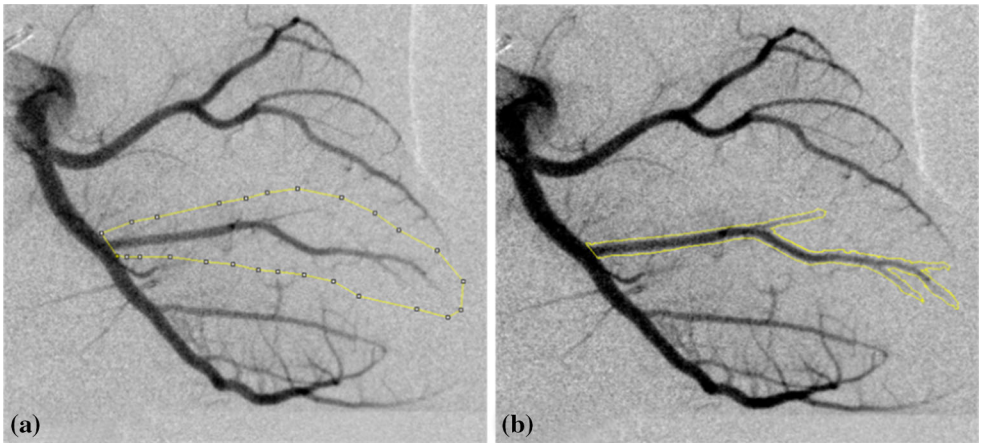

Fig. 1 ROIs of coronary blood flow and volume measurements. An example of a region-of-interest (ROI) used for angiographically measured coronary volumetric flow (**a**), and epicardial arterial volume (**b**) determination in branch

CFR_a, $rCFR_a$, and FFR_a measurement

Absolute CFR is defined as the ratio of blood flow at maximum hyperemia to the baseline flow. Thus the angiography based CFR (CFR_a) can be calculated using the angiographic flow based on the FPA technique as shown in Eq. (1).

$$CFR_a = \frac{Q_{target-hyperemia}}{Q_{target-baseline}} \quad (1)$$

Relative angiographic CFR ($rCFR_a$) is defined as the ratio of the hyperemic flow in a target artery to another normal artery as shown in Eq. (2).

$$rCFR_a = \frac{Q_{target-hyperemia}}{Q_{reference-hyperemia}} \quad (2)$$

FFR is defined as the hyperemic flow through a target artery divided by the hypothetical normal hyperemic flow through the same artery without disease. The flow of the target diseased artery ($Q_{target\text{-}hyperemia}$) could be directly measured by using FPA technique. However, the hypothetical normal hyperemic flow is not known. Previous studies [7, 10] have shown that a power law relationship exists between the hyperemic blood flow (Q_{normal}) through a stem and its corresponding crown volume (V):

$$Q_{normal} = k\left(\frac{V}{V_{ref}}\right)^{3/4} \quad (3)$$

k is the scaling coefficient. V_{ref} (1 ml) is a reference volume to make V raised to the power of 3/4 unitless. The hypothetical normal hyperemic coronary blood flow (Q_{normal}) could be calculated from the corresponding crown volume (V) by using Eq. (3). Therefore, angiographic FFR (FFR_a) can then be calculated using:

$$FFR_a = \frac{Q_{target-hyperemia}}{k\left(\frac{V}{V_{ref}}\right)^{3/4}} \quad (4)$$

This equation shows that FFR_a can be measured using $Q_{target\text{-}hyperemia}$, V and k. A technique to measure lumen volume using angiographic image data has also been validated [3, 4]. Pressure-derived FFR (FFR_P) is calculated according to the following expression using aortic pressure (P_a), the coronary pressure distal to the stenosis (P_d) and coronary back pressure (P_v):

$$FFR_P = \frac{P_d - P_v}{P_a - P_v} \quad (5)$$

FFR_P was calculated from mean pressure values over five cardiac cycles just prior to coronary angiography.

Diagnosis for both epicardial stenosis and microcirculation disruption

The diagnostic abilities for target artery were assessed in three models: (1) the epicardial stenosis model (S), which included normal conditions and various degrees of epicardial stenoses without any microsphere injection; (2) the microcirculation disruption model (M), which included normal conditions and different severities of microvascular disruptions with normal epicardial arteries; and (3) the combined (S + M) model, which had various degrees coronary epicardial stenoses with different severities of microvascular disruption. The disease vessels were defined as FFR <0.8 (stenosis) and/or microsphere injection (ml)/arterial lumen volume (ml) >4 [9, 11], with CFR <2.0.

Statistical analysis

Linear regression analysis was performed among the angiographic FFR_a and pressure derived FFR_p measurement to

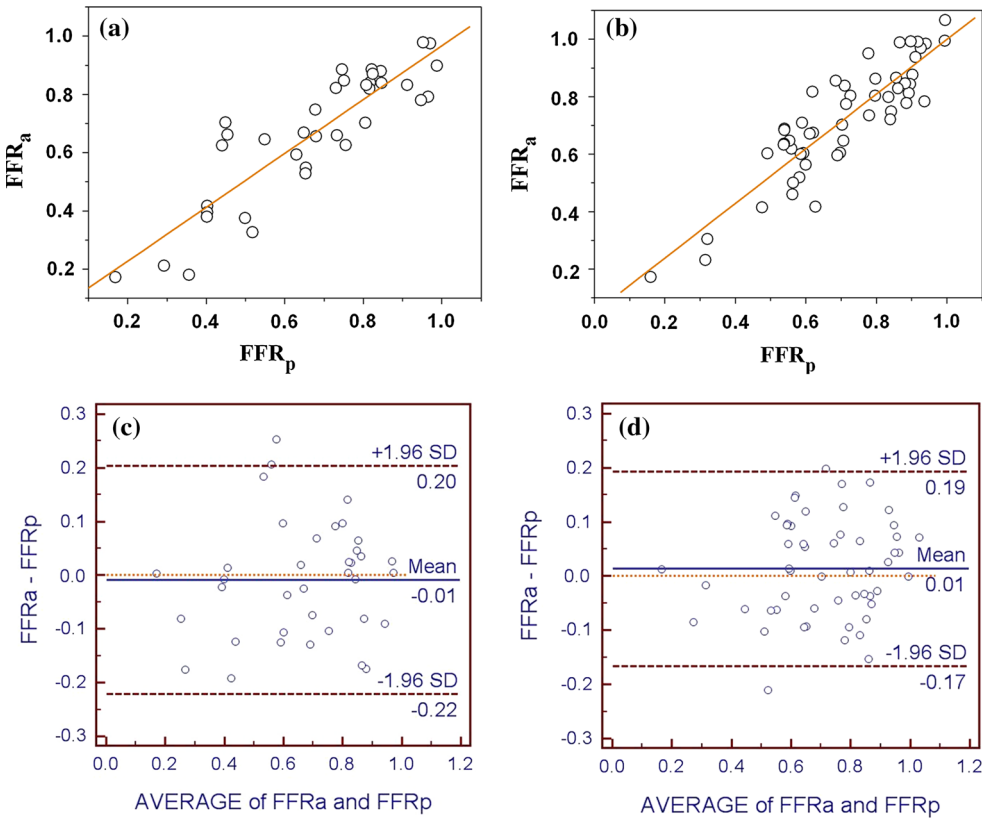

Fig. 2 Comparison between $FFR_a$and FFR_p measurements. A linear regression analysis (**a**, **b**) and the Bland–Altman analysis (**c**, **d**) of angiographic FFR (FFR_a) and the pressure derived FFR (FFR_p) measurements. (**a** S model: $FFR_a = 0.92\ FFR_p + 0.04$, N = 37, r = 0.88, SEE = 0.11, $p < 0.0001$; **b** M model $FFR_a = 0.95\ FFR_p + 0.05$, N = 53, r = 0.89, SEE = 0.09, $p < 0.0001$). Additionally, in a Bland–Altman plot, the mean differences between FFR_p and FFR_a measurements were -0.01 ± 0.21 in the S model (**c**) and 0.01 ± 0.18 in M model (**d**)

determine the correlation coefficient (r) and standard error of estimate (SEE). SEE defines the standard deviation of the measured values from the regression line. The degree of agreement between the different methods was also assessed in the Bland–Altman analysis. Paired student's *t* test was used to compare the angiographic indices (CFR_a, $rCFR_a$, and FFR_a) between the disease and normal vessels. Receiver operating characteristic (ROC) curves were made for CFR_a, $rCFR_a$ and FFR_a measurements in S, M and S + M models. The areas under each curve (AUC) were calculated to compare the diagnostic abilities of the different indices. A $p < 0.05$ was considered to be statistically significant for all statistical analyses.

Results

Comparison between the angiographic FFR and the pressure-derived FFR

Among all the measurements, there were only 37 pairs of FFR measurements for both FFR_a and FFR_p in S model, and 53 pairs in M model (diameters from 1.7 to 4.21 mm). FFR_a correlated linearly with FFR_p with a good correlation coefficient in both S and M models (S model: $FFR_a = 0.92\,FFR_p + 0.04$, r = 0.88, SEE = 0.11, $p < 0.001$; M model: $FFR_a = 0.95\ FFR_p + 0.05$, r = 0.89, SEE = 0.09, $p < 0.001$). Additionally, in a Bland–Altman plot, the mean differences between FFR_p and FFR_a measurements were -0.01 ± 0.21 in the S model and 0.01 ± 0.18 in the M model (Fig. 2).

Table 1 Comparison of CFR and FFR measurements in normal and diseased arteries including the main trunk and braches of coronary arteries

Indices	Normal arteries (n)	Disease arteries (n)	*p*
CFR_a	2.170 ± 0.746 (212)	1.823 ± 0.489 (89)	0.000*
$rCFR_a$	1.043 ± 0.182 (17)	0.623 ± 0.212 (19)	0.000*
FFR_a	0.952 ± 0.174 (212)	0.619 ± 0.205 (89)	0.000*

* There were significant differences between the normal and disease arteries

Hemodynamic indices comparison between normal and disease arteries

There were a total of 301 blood flow measurements in the main and branches of coronary arteries both at baseline and maximum hyperemia. From the student *t* test, there were significant differences between the normal (n = 212) and disease arteries (n = 89) for all the indices (Table 1). All the hemodynamic indices could be calculated by using the angiographic image data in a large diameter range of

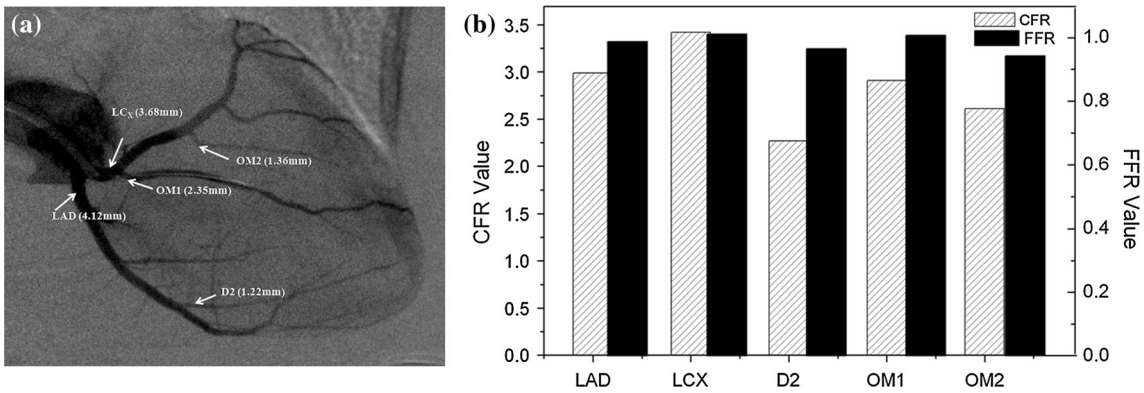

Fig. 3 An example of FFR_a and CFR_a in the trunk and branches of coronary arteries in one individual animal. The figure showed that the hemodynamic indices can be calculated by using the angiographic image data for a large diameter range of 4.12–1.22 (mm). Left anterior descending artery—LAD, left circumflex artery—LC_X, second diagonal branch—D2, obtuse marginal branch—OM

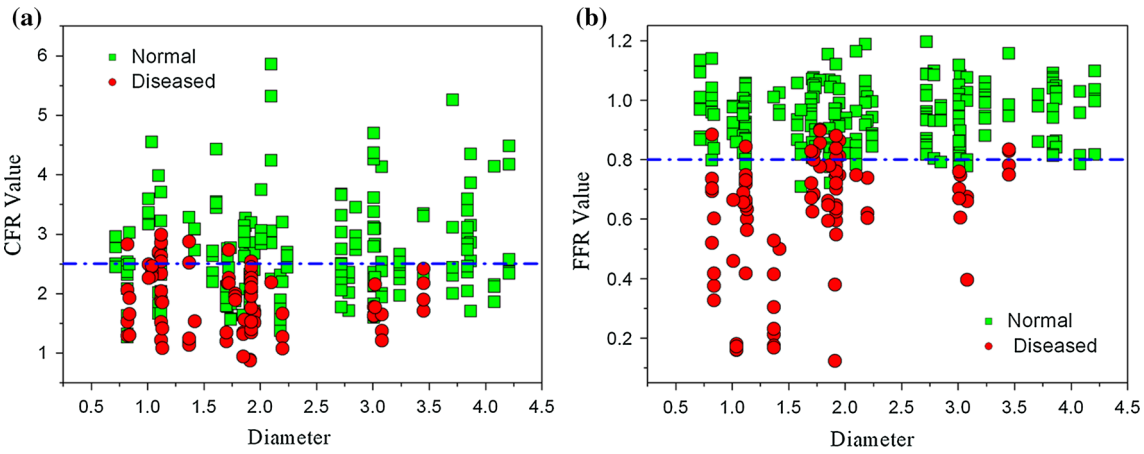

Fig. 4 The distribution of the normal and disease CFR and FFR values in a large range of artery sizes for all the models. The figure shows the distribution of CFR and FFR in the diameter range of 4.21–0.72 mm. Cut-off values of 2.5 and 0.8 can be used for CFR and FFR respectively, to distinguish the normal and the diseased conditions

0.72–4.21 mm. Figure 3 shows an example of FFR_a and CFR_a in the main coronary artery and its branches in one animal. Figure 4 shows a distribution of CFR and FFR in the diameter range of 0.72–4.21 mm in all the measurements. A cut-off value of 0.8 can be used for FFR to distinguish the normal and the diseased conditions.

The diagnostic abilities for culprit vessels

From 225 measurements made using the S model (212 normals vs. 13 stenoses), the AUCs for CFR_a and FFR_a were 0.720 and 0.918 ($p < 0.05$), respectively (Fig. 5a). There was not enough data for $rCFR_a$ in the S Model. From 262 measurements made using the M model (212 normal arteries vs. 50 microvascular disruptions), the AUCs were 0.744, 0.715, and 0.959 for CFR_a, $rCFR_a$ and FFR_a ($p < 0.05$), respectively (Fig. 5b). Additionally, in the 238 measurements of the S + M model (212 normal vs. 26 stenoses with microvascular disruption), the AUCs for CFR_a, $rCFR_a$ and FFR_a were 0.806, 0.738, and 0.995 ($p < 0.05$) (Fig. 5c). All the angiographic indices can be used to diagnose the culprit vessels, and FFR_a had the highest AUCs among the three. The sensitivities and specificities of the best cut-off values for all the hemodynamic indices are listed in Table 2.

Discussion

Previous studies have validated that angiographic hemodynamic indices can be accurately measured using the FPA technique [4, 7]. The present study demonstrated that FFRa based on the FPA technique strongly correlates with the reference FFR_p from pressure wire in both proximal segment and branches of coronary arterial trees. CFR_a, $rCFR_a$ and FFR_a of the branches were compared in stenosis (S),

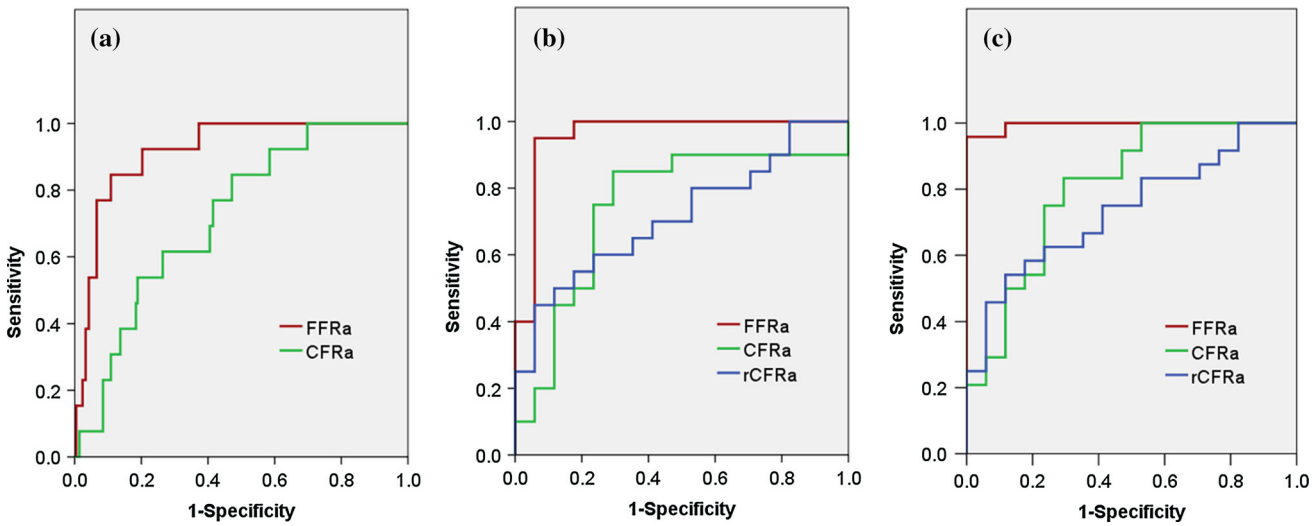

Fig. 5 The ROC curves to detect stenosis and the microvascular disease. **a** S model: stenosis group versus normal group (AUC: $FFR_a = 0.918$, $CFR_a = 0.720$, n = 225, $p < 0.05$), **b** M model: microvascular disease group versus Normal group (AUC: $FFR_a = 0.959$, $CFR_a = 0.744$, $rCFR_a = 0.715$, n = 262, $p < 0.05$), **c** S + M model: complicated disease group versus normal group (AUC: $FFR_a = 0.995$, $CFR_a = 0.806$, $rCFR_a = 0.738$, n = 238, $p < 0.05$)

microvascular disruption (M), and combined (S + M) models. The results showed that FFR_a was a promising index to determine the culprit coronary arterial branches.

Comparison of different hemodynamic indices

Absolute CFR_a's application is hampered by the unknown baseline hemodynamic loading condition and variability between the inter-study of normal values [12, 13]. In the current study, the FFR values were almost close to 1.0 in the normal condition, while the range of CFR values were from 1.5 to 6.0, which may be due to the unstable hemodynamic condition of the normal arteries. $rCFR_a$ can overcome some of the limitations of absolute CFR_a by using a normal artery of the same size as a Ref. [3], However, in a patient-specific scenario, a similar sized reference artery might not be available. Even in the case where the diameter of the artery might be similar, the perfusion bed of the target and reference arteries may be different. FFR_a can be widely applied to both the main coronary arteries and their branches regardless of the arterial distribution and lesions. FFR_a also has a normal value of 1.0, which is not influenced by the unknown baseline conditions [2, 14]. The current results show that FFR_a is the most accurate and reliable diagnostic index among the three indices evaluated in all the disease models.

Among coronary hemodynamic indices, FFR is a lesion-specific parameter, while CFR characterizes the entire vascular tree [15]. Hence, simultaneous measurement of CFR and FFR may allow us to estimate the lesion severity along with an assessment of the vascular bed's perfusion condition.

Angiographic hemodynamic indices in small arterial branches

FFR_p is currently being used to assess lesions with intermediate severity. However, it is difficult to make pressure wire measurement in small arterial branches, especially when more than one branch could be the culprit. Angiographic hemodynamic indices based on FPA technique can potentially overcome this limitation [3, 4]. In the current study, CFR_a, $rCFR_a$, and FFR_a could be measured in a large diameter range of 0.72–4.21 mm. Figure 4 shows that the generally used cut-off values for CFR and FFR could potentially be used to distinguish between the normal and the diseased arteries even in the small branches. The ROCs of CFR_a, $rCFR_a$, and FFR_a in the three different disease models had similar AUCs, sensitivities, and specificities as compared to a previous study on the LAD of a swine animal model [3, 9]. As compared to our previous FFR validation studies, the current study focused on the small branches instead of the main coronary arteries. Additionally, the current study used a heparin-coated polyurethane tubing to create a local stenosis in a closed chest swine model.

Future clinical applications and angiographic hemodynamic map

By using the conventional coronary angiographic images, it is potentially possible to get basic physiological information for every point in the entire coronary artery tree. The overall information about the proximal and branches of coronary arteries could be present in angiographic

Table 2 Comparison of diagnostic ability of the hemodynamic indices indifferent disease models

	S Model (n = 225)				M Model (n = 262)				S + M Model (n = 238)			
	AUC	Sensitivity	Specificity	95 % confidence	AUC	Sensitivity	Specificity	95 % confidence	AUC	Sensitivity	Specificity	95 % confidence
CFRa	0.720	0.615	0.736	0.601 0.839	0.744	0.850	0.706	0.573 0.916	0.806	0.833	0.706	0.666 0.947
rCFRa	–	–	–	– –	0.715	0.600	0.765	0.549 0.880	0.738	0.625	0.765	0.587 0.889
FFRa	0.918	0.846	0.892	0.859 0.977	0.959	0.950	0.941	0.000 1.000	0.995	0.958	1.000	0.000 1.000

hemodynamic maps. Figure 6 shows an example of determining the culprit coronary branch with measured FFR_a in different branches of coronary arterial tree. Theoretically, different types of hemodynamic maps, such as normalized flow, CFR_a, $rCFR_a$, FFR_a, and normalized microvascular resistance (NMR) could be calculated by using the same angiographic image data [9, 11]. Combined use of different hemodynamic maps can potentially provide the possibility to determine the flow impairment in both the main coronary arteries and their branches in order to detect/locate the culprit artery. Additionally, FFR_a can potentially be applied in some special circumstances in which pressure wire cannot be used such as tortuous vessels, distal blood vessels and side branch after stent implantation [16].

Microcirculation reaction-FFR_p and FFR_{CT}

The value of FFR is influenced not only by stenosis severity, but also by the amount of viable myocardium subtended by the epicardial coronary arterial branch harboring the stenosis. In our previous study, FFR_p overestimated the measurement using reference standard flow-probe FFR, especially at low values [17]. The current results improved the Y-intercept to $\sim$0.05 by maintaining the blood pressure for the whole experiment; however, the FFR_p was still lower than FFR_a at low pressure values ($\sim$0.4 mmHg). Pijls et al. [1] showed that with increasing stenosis severity the coronary flow ratio progressively underestimated the pressure-based index. Siebes and Spaan et al. [12, 18] demonstrated the curved nature of pressure-flow relations and how this shape relates to the pressure dependence of minimal coronary microvascular resistance.

Another recent new concept-FFR_{CT}, which is calculated based on computational fluid dynamics (CFD) theory by using computed tomography angiography (CTA) images only, has shown the diagnostic accuracy of noninvasive FFR measurement in order to determine the presence of ischemia-inducing coronary lesions by reducing the false positive rate [19]. However, FFR_{CT} is calculated during simulated hyperemia by assuming that microcirculation reacts predictably to maximal hyperemic conditions in patients with normal coronary artery flow. Just similar to the CFR measurement error, the arteriole and microcirculation reactions may be variable to the vasodilators.

As Gould et al. [20] have previously summarized, an inaccurate physiological prediction can result from two general reasons. (1) Input parameter may contain uncertainty, like the simulated parameters; (2) the predictive model may contain inaccurate blood flow due to microvascular disease. A reduction of coronary blood flow, which may be caused by an epicardial coronary stenosis or increasing resistance of microcirculation, will affect the profile, perfusion, and wash-out in angiography because

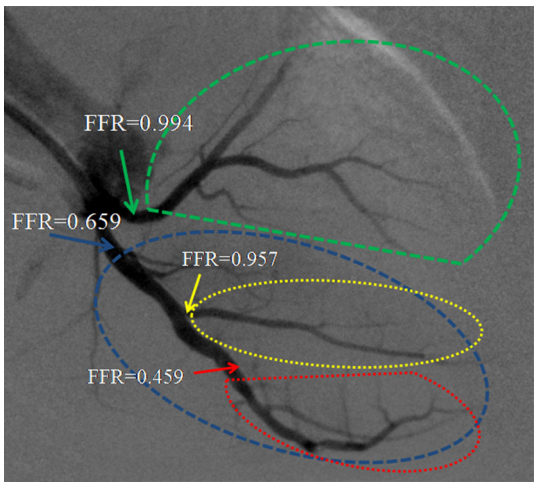

Fig. 6 Anexample of application for angiographic FFR_a. All arteries (~0.7 mm in diameter) can be measured by using angiography, but the FFR_a may have the potential to detect the diseased artery or locate the ischemia producing region of the coronary arterial tree

angiography contains both anatomical and physiological information [21]. It may be difficult to evaluate the physiological significance of stenosis and to distinguish the abnormalities of micro-circulation by only using FFR_a [9]. However, a combination of different angiographic indices such as CFR_a, $rCFR_a$ and FFR_a, normalized flow, especially NMR can potentially provide a more accurate physiological prediction by avoiding the previously mentioned significant errors [3, 9].

Study limitation

First, coronary flow and volume measurement errors in the small branches may be higher than in the entire LAD or LC_X because of the reduced flow and angiographic resolution. In the current close chest animal model, it was not possible to place flow probe on the small branches to measure the flow for CFR validation. The results showed a variance of approximately 0.2 in FFR_a, which is too high for clinical application. Therefore, additional optimization of the methodology is necessary before its clinical implementation. Second, other disease conditions, such as ventricular hypertrophy, diffuse coronary artery disease, and prior myocardial infarction have their own physiological and pathological characteristics that may have potential impacts on the angiographic hemodynamic index measurements. Third, 1–2 % isoflurane may cause coronary vasodilatation in the rest condition for some animals. Furthermore, the animals become unstable over time, which might be one reason for the high variability in FFR_a measurements. Fourth, the current study was only performed on the LAD and LCX. The pressure in the right ventricle is remarkably lower compared to that of the left ventricle. Therefore more detailed validation on the RCA is also necessary. Future studies will investigate the hemodynamic differences including pressure, flow, CFR, FFR and NMR, between the left and right coronary arteries.

Conclusions

This study demonstrated that hemodynamic indices such as CFR_a, $rCFR_a$ and FFR_a could potentially be measured in small coronary arterial branches (down to ~0.7 mm) by using the FPA technique from angiographic images. This technique is easy to perform, requiring only angiographic images.

Acknowledgments The authors would like to thank Drs. Jerry Wong and Charles Dang for their technical support. We would like to acknowledge partial funding for Zhang Zhang from China National Natural Science Foundation Grant 81301217 and 81301202. This work was supported in part by the National Heart, Lung and Blood Institute and the Department of Health and Human Services [R01 HL89941].

Conflict of interest No conflicts to disclose.

References

1. Pijls NH, Sels JW (2012) Functional measurement of coronary stenosis. J Am Coll Cardiol 59(12):1045–1057. doi:10.1016/j.jacc.2011.09.077
2. Yong AS, Daniels D, De Bruyne B, Kim HS, Ikeno F, Lyons J, Pijls NH, Fearon WF (2013) Fractional flow reserve assessment of left main stenosis in the presence of downstream coronary stenoses. Circ Cardiovasc Interv 6(2):161–165. doi:10.1161/CIRCINTERVENTIONS.112.000104
3. Zhang Z, Takarada S, Molloi S (2012) Quantification of absolute coronary flow reserve and relative fractional flow reserve in a swine animal model using angiographic image data. Am J Physiol Heart Circ Physiol 303(3):H401–H410. doi:10.1152/ajpheart.00153.2012
4. Takarada S, Zhang Z, Molloi S (2013) An angiographic technique for coronary fractional flow reserve measurement: in vivo validation. Int J Cardiovasc Imaging 29(3):535–544. doi:10.1007/s10554-012-0119-0
5. Carlsson M, Saloner D, Martin AJ, Ursell PC, Saeed M (2010) Heterogeneous microinfarcts caused by coronary microemboli: evaluation with multidetector CT and MR imaging in a swine model. Radiology 254(3):718–728. doi:10.1148/radiol.09090527
6. Molloi S, Kassab GS, Zhou Y (2001) Quantification of coronary artery lumen volume by digital angiography: in vivo validation. Circulation 104(19):2351–2357
7. Wong JT, Molloi S (2008) Determination of fractional flow reserve (FFR) based on scaling laws: a simulation study. Phys Med Biol 53(14):3995–4011. doi:10.1088/0031-9155/53/14/017
8. Molloi S, Chalyan D, Le H, Wong JT (2012) Estimation of coronary artery hyperemic blood flow based on arterial lumen volume using angiographic images. Int J Cardiovasc Imaging 28(1):1–11. doi:10.1007/s10554-010-9766-1

9. Zhang Z, Takarada S, Molloi S (2011) Assessment of coronary microcirculation in a swine animal model. Am J Physiol Heart Circ Physiol 301(2):H402–H408. doi:10.1152/ajpheart.00213.2011
10. Zhang Z, Molloi S (2013) A novel angiographic fractional flow reserve. Reply. Am J Physiol Heart Circ Physiol 304(8):H1176–H1177. doi:10.1152/ajpheart.00136.2013
11. Zhang Z, Takarada S, Molloi S (2011) Quantification of coronary microvascular resistance using angiographic images for volumetric blood flow measurement: in vivo validation. Am J Physiol Heart Circ Physiol 300(6):H2096–H2104. doi:10.1152/ajpheart.01123.2010
12. Spaan JA (2009) Coronary flow is not that simple! Heart 95(9):761–762 (author reply 762)
13. Gould KL, Lipscomb K, Hamilton GW (1974) Physiologic basis for assessing critical coronary stenosis: instantaneous flow response and regional distribution during coronary hyperemia as measures of coronary flow reserve. Am J Cardiol 33(1):87–94
14. De Bruyne B, Sarma J (2008) Fractional flow reserve: a review: invasive imaging. Heart 94(7):949–959. doi:10.1136/hrt.2007.122838
15. Pawlowski T, Prati F, Kulawik T, Ficarra E, Bil J, Gil R (2013) Optical coherence tomography criteria for defining functional severity of intermediate lesions: a comparative study with FFR. Int J Cardiovasc Imaging 29(8):1685–1691. doi:10.1007/s10554-013-0283-x
16. Mittal N, Zhou Y, Ung S, Linares C, Molloi S, Kassab GS (2005) A computer reconstruction of the entire coronary arterial tree based on detailed morphometric data. Ann Biomed Eng 33(8):1015–1026. doi:10.1007/s10439-005-5758-z
17. Spaan JAE, Piek JJ, Hoffman JIE, Siebes M (2006) Physiological basis of clinically used coronary hemodynamic indices. Circulation 113(3):446–455. doi:10.1161/Circulationaha.105.587196
18. Siebes M, Verhoeff BJ, Meuwissen M, de Winter RJ, Spaan JAE, Piek JJ (2004) Single-wire pressure and flow velocity measurement to quantify coronary stenosis hemodynamics and effects of percutaneous interventions. Circulation 109(6):756–762. doi:10.1161/01.Cir.0000112571.06979.B2
19. Min JK, Leipsic J, Pencina MJ, Berman DS, Koo BK, van Mieghem C, Erglis A, Lin FY, Dunning AM, Apruzzese P, Budoff MJ, Cole JH, Jaffer FA, Leon MB, Malpeso J, Mancini GB, Park SJ, Schwartz RS, Shaw LJ, Mauri L (2012) Diagnostic accuracy of fractional flow reserve from anatomic CT angiography. JAMA 308(12):1237–1245. doi:10.1001/2012.jama.11274
20. Johnson NP, Kirkeeide RL, Gould KL (2013) Coronary anatomy to predict physiology: fundamental limits. Circ Cardiovasc Imaging 6(5):817–832. doi:10.1161/CIRCIMAGING.113.000373
21. Wu Z, Ye F, You W, Zhang J, Xie D, Chen S (2014) Microcirculatory significance of periprocedural myocardial necrosis after percutaneous coronary intervention assessed by the index of microcirculatory resistance. Int J Cardiovasc Imaging. doi:10.1007/s10554-014-0444-6